Table II. Least-Squares-Refined Parameters and Estimated Standard Deviations (in Parentheses)[a] from Best Fits of Eq 1 to EXAFS Spectra of $SmNb_3Cl_{14}$ and Nb_2Cl_{10}

		best-fit parameters				model-adjusted results[b]		expected[c] results		
compd	term	ΔE_0, eV	r, Å	σ, Å	B	r, Å	N	r, Å	N(I)	N(II)
$SmNb_3Cl_{14}$	Nb–Cl_{ter}	−0.93	2.309 (15)	0.097 (7)	2.61	2.324 (8)	3.2 (7)	2.30	3.33	2.00
	Nb–Cl_{br}	−10.87	2.509 (15)	0.048 (39)	0.87	2.552 (25)	2.4 (20)[d]	2.42–2.55	2.67	4.00
	Nb–Nb	−5.70	3.051 (19)	0.043 (31)	0.14	3.042 (9)	0.7 (4)	3.03	1.33	1.33
Nb_2Cl_{10}	Nb–Cl_{ter}	−0.82	2.263 (7)	0.037 (15)	1.30			2.302 (5)	4	
	Nb–Cl_{br}	−7.06	2.544 (29)	0.070[e]	0.59			2.555 (6)	2	
	Nb–Nb	−9.54	3.935 (17)	0.079 (16)	0.52			3.951 (2)	1	

[a] Standard deviations were estimated as in ref 10d and do not include possible systematic errors. [b] The best-fit values of r were corrected by the FABM method as described by Teo et al.[10d] The coordination numbers N were calculated from the best-fit values of B by using amplitude reduction factors S obtained from the B(Nb–Cl_{ter}) and B(Nb–Nb) vs. σ correlation curves of Nb_2Cl_{10} at the best-fit σ values for $SmNb_3Cl_{14}$. [c] For $SmNb_3Cl_{14}$ the expected values refer to structures I and II; the X-ray results for Nb_2Cl_{10} are from ref 16. [d] The very large uncertainty of this result is due to the insensitivity of the fit to the values of the strongly coupled parameters σ_{br} and B_{br}. [e] The fit is extremely insensitive to the value of this Debye–Waller factor; it was held fixed at the value calculated[10c] from the Nb–Cl_{br} stretching frequency (248 cm^{-1}).

A nonlinear least-squares procedure[13] was used to fit the Fourier-filtered, truncated $\mathbf{k}^3[\chi(\mathbf{k})]$ vs. $\mathbf{k}$ EXAFS data[12] with the single scattering short-range order theory equation[10,14]

$$\mathbf{k}^3[\chi(\mathbf{k})] = \sum_j B_j[F_j(\mathbf{k}_j)]\mathbf{k}_j^2 \exp(-2\sigma_j^2\mathbf{k}_j^2) \sin [2\mathbf{k}_j r_j + \phi_j(\mathbf{k}_j)]/r_j^2 \quad (1)$$

where $F_j(\mathbf{k}_j)$, $\phi_j(\mathbf{k}_j)$, σ_j, r_j, and $\mathbf{k}_j$ represent the backscattering amplitude, the total photoelectron phase shift, the Debye–Waller factor, the distance from the absorbing atom, and the photoelectron wave vector, respectively, for a neighboring atom of type j. B_j is a scale factor related to N_j, the number of j-type neighbor atoms, by $N_j = B_j/S_j$; the amplitude reduction factor S_j was evaluated from the model compound EXAFS spectrum. $F_j(\mathbf{k}_j)$ and $\phi_j(\mathbf{k}_j)$ were fixed at their theoretical values during the least-squares fitting.[15] Wave vectors $\mathbf{k}$ and $\mathbf{k}_j$ are related by[15]

$$\mathbf{k}_j = (\mathbf{k}^2 - 2(\Delta E_{0j})/7.62)^{1/2}$$

where $\Delta E_{0j} = E_{0j}^{theor} - E_0^{exptl}$ is the difference between the experimental absorption edge threshold energy[11] and the threshold energy for which the theoretical $\phi_j(\mathbf{k}_j)$ function is defined. There are therefore four parameters, r_j, ΔE_{0j}, σ_j, and B_j, to be least-squares refined for each term of eq 1. Figure 1b shows the Fourier-filtered Nb–Cl EXAFS spectrum and the least-squares fit to eq 1 with two terms. The Nb–Nb peak was filtered and fit with one term of eq 1. Table II summarizes the results of the least squares analyses.

The results in Table II are consistent with the formulation $Sm^{3+}[Nb_3Cl_{14}]^{3-}$ and a structure comprised of a chain of three $NbCl_6$ octahedra sharing common edges (I). They are also

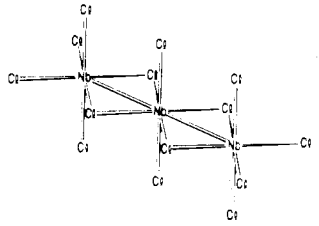

I

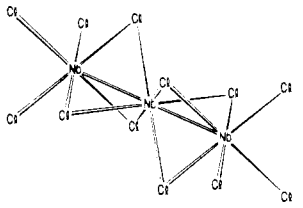

II

consistent with the formulation $Sm^{3+}[Nb_3Cl_{12}]^-Cl^-_2$ and a structure comprised of a chain of three $NbCl_6$ octahedra sharing common faces (II). The short Nb–Nb bond accounts for the diamagnetism of $[Nb_3Cl_{14}]^{3-}$ or $[Nb_3Cl_{12}]^-$, which may be represented as containing Nb in the oxidation states IV(d^1)–III(d^2)–IV(d^1) with the spins paired in $\sigma^2\pi^2$ metal–metal bonds. Each Nb–Nb pair has a bond order of 1, consistent with the observed Nb–Nb distance. A triangular $[Nb_3Cl_{12}]^-$ cluster would have a bond order of $^2/_3$ and would be expected to have a longer Nb–Nb distance than is observed. The $[Nb_3Cl_{14}]^{3-}$ structure is related to the structure of $NbCl_4$.[17] The latter compound contains linear chains of edge-sharing $NbCl_6$ octahedra in which long (3.794 (2) Å) and short (3.029 (2) Å) Nb–Nb distances alternate; the bonded Nb–Nb pairs are linked by a single σ bond. Although the short Nb–Nb distance in $NbCl_4$ is close to the distance in $[Nb_3Cl_{14}]^{3-}$, the corresponding Nb–Cl_{br} distance (2.425 (1) Å) is significantly shorter than this distance in $[Nb_3Cl_{14}]^{3-}$.[18] The Nb–Cl_{ter} distance in $[Nb_3Cl_{14}]^{3-}$ is significantly longer than the distance in $NbCl_4$ (2.291 (2) Å). However, we note that there is probably an appreciable spread between nonequivalent Nb–Cl_{ter} distances. This is indicated by the large value found for the Debye–Waller factor of the Nb–Cl_{ter} bond, which suggests a distance spread of ~0.1 Å[10c,19] and the possibility of significant Sm–Cl interactions.

Acknowledgment. We are very much indebted to Dr. B. K. Teo for educating us in the art of measuring and analyzing EXAFS spectra. We thank Prof. D. F. Shriver for his help and Peter Blonsky for his aid in operating the EXAFS spectrometer.

(13) A Bell Labs fitting program based on Marquardt's method.
(14) Stern, E. A. *Phys. Rev. B: Solid State* **1974**, *10*, 3027. Lee, P. A.; Pendry, J. B. *Phys. Rev. B: Solid State* **1975**, *11*, 2795. Lee, P. A.; Beni, G. *Phys. Rev. B: Solid State* **1977**, *15*, 2862.
(15) Teo, B. K.; Lee, P. A. *J. Am. Chem. Soc.* **1979**, *101*, 2815.
(16) Zalkin, A.; Sands, D. E. *Acta Crystallogr.* **1958**, *11*, 615.
(17) Taylor, D. R.; Calabrese, J. C.; Larsen, E. M. *Inorg. Chem.* **1977**, *16*, 721.
(18) The corresponding Cl_{br}–Nb–Cl_{br} angles are 106.8° in $[Nb_3Cl_{14}]^{13-}$ and 102.7° in $NbCl_4$.
(19) Teo, B. K.; Shulman, R. G.; Brown, G. S.; Meixner, A. E. *J. Am. Chem. Soc.* **1979**, *101*, 5624.

Contribution from the Department of Chemistry, University of Virginia, Charlottesville, Virginia 22901

Solvent-Induced ^{11}B NMR Shifts in Metallaboranes and Metallacarboranes

T. Leon Venable,[1a] Cynthia T. Brewer,[1b] and Russell N. Grimes*

Received March 26, 1985

Although the effect of solvent on proton NMR spectra of boron cage compounds has been examined,[2] and Onak et al. have correlated solvent shifts with proton charges,[2a] the ^{11}B NMR spectra of polyhedral boranes and carboranes are usually assumed to be negligibly affected by the choice of solvent, with observed solvent shifts normally much less than 1 ppm and measurable only on high-resolution instruments.[3] A recently noted exception[4] is

(1) (a) Present address: Department of Chemistry, Agnes Scott College, Decatur, GA 30030. (b) Excerpted in part from: Brewer, C. T. Ph.D. Thesis, University of Virginia, 1984.
(2) (a) Onak, T.; Inman, W.; Rosendo, H.; DiStefano, E. W.; Nurse, J. *J. Am. Chem. Soc.* **1977**, *99*, 6488. (b) Jarvis, W.; Inman, W.; Powell, B.; DiStefano, E. W.; Onak, T. *J. Magn. Reson.* **1981**, *43*, 302.

0020-1669/85/1324-4751$01.50/0

Table I. Solvent-Induced ^{11}B FT NMR Shifts for 2,3-$(C_2H_5)_2C_2B_4H_6$

solvent	δ[B(5)][a]	$\Delta\delta$[b]	δ[B(4,6)]	$\Delta\delta$	δ[B(1)]	$\Delta\delta$
hexane	−1.3		−4.2		−47.5	
toluene	−1.7	−0.4	−4.6	−0.4	−47.7	−0.2
diethyl ether	−1.0	+0.3	−4.1	+0.1	−47.3	+0.2
tetrahydrofuran	−1.6	−0.3	−4.6	−0.4	−47.6	−0.1
acetone	−0.8	+0.5	−4.1	+0.1	−47.1	+0.4
dichloromethane	−1.6	−0.3	−4.3	−0.1	−47.8	−0.3
ethanol	−1.2	+0.1	−4.4	−0.2	−47.5	0.0
acetonitrile	−0.9	+0.4	−4.2	0.0	−47.4	+0.1
		+0.4 (av)		−0.1 (av)		0.0

[a] Chemical shifts relative to external $BF_3{\cdot}O(C_2H_5)_2$. [b] $\Delta\delta = \delta_{solvent} - \delta_{hexane}$.

Table II. Solvent-Induced ^{11}B FT NMR Shifts for 1,2,3-$LFe(C_2H_5)_2C_2B_4H_4$

solvent	δ[B(4,6)]	$\Delta\delta$	δ[B(5 or 7)][a]	$\Delta\delta$	δ[B(7 or 5)][a]	$\Delta\delta$
			L = η^6-C_6H_6			
hexane	2.7		9.5		8.1	
benzene	2.0	−0.7	8.0	−1.5	6.7	−1.4
diethyl ether	2.3	−0.4	8.3	−1.2	6.9	−1.2
tetrahydrofuran	1.6	−1.1	7.2	−2.3	5.7	−2.4
acetone	2.2	−0.5	7.3	−2.2	5.8	−2.3
dichloromethane	1.4	−1.3	5.9	−3.6	5.6	−2.5
chloroform	1.5	−1.2	5.9	−3.6	5.9	−2.2
		−0.9 (av)		−2.4 (av)		−2.0 (av)
			L = η^6-C_8H_{10}			
hexane	3.8		13.4		7.8	
benzene	3.2	−0.6	12.1	−1.3	6.6	−1.2
diethyl ether	3.6	−0.2	12.7	−0.7	7.0	−0.8
tetrahydrofuran	3.4	−0.4	12.1	−1.3	6.4	−1.4
acetone	3.5	−0.3	11.6	−1.8	6.0	−1.8
dichloromethane	2.6	−1.2	10.2	−3.2	5.4	−2.4
chloroform	2.7	−1.1	10.3	−3.1	5.9	−1.9
methanol	2.6	−1.2	10.3	−3.1	5.5	−2.3
acetonitrile	3.6	−0.2	11.2	−2.2	5.9	−1.9
		−0.7 (av)		−2.1 (av)		−1.7 (av)

[a] Assignment of the B(5) and B(7) resonances is ambiguous.

Table III. Solvent-Induced ^{11}B FT NMR Shifts for 1,2,3-$(\eta^8$-$C_8H_8)Ti(C_2H_5)_2C_2B_4H_4$

solvent	δ[B(4,6)]	$\Delta\delta$	δ[B(5)]	$\Delta\delta$	δ[B(7)]	$\Delta\delta$
benzene	16.9		24.3		−21.1	
diethyl ether	17.2	+0.3	24.7	+0.4	−21.0	+0.1
tetrahydrofuran	16.4	−0.5	23.0	−1.3	−21.8	−0.7
acetone	16.7	−0.2	23.1	−1.2	−21.6	−0.5
dichloromethane	15.9	−1.0	21.8	−2.5	−22.2	−1.1
chloroform	16.1	−0.8	21.9	−2.4	−22.0	−0.9
methanol	15.6	−1.3	21.1	−3.2	−22.5	−1.4
acetonitrile	16.2	−0.7	21.9	−2.4	−22.1	−1.0
		−0.6 (av)		−1.7 (av)		−0.8 (av)

Table IV. Solvent-Induced ^{11}B FT NMR Shifts for 2-$(\eta^5$-$C_5H_5)CoB_4H_8$

solvent	δ[B(1)]	$\Delta\delta$	δ[B(3,5)]	$\Delta\delta$	δ[B(4)]	$\Delta\delta$
hexane	−11.2		−15.0		10.4	
benzene	−12.9	−1.7	−14.8	+0.2	9.2	−1.2
diethyl ether	−12.8	−1.6	−14.8	+0.2	9.2	−1.2
tetrahydrofuran	−14.6	−3.4	−14.6	+0.4	8.3	−2.1
acetone	−14.1	−2.9	−14.1	+0.9	8.5	−1.9
dichloromethane	−14.8	−3.6	−14.8	+0.2	8.3	−2.1
methanol	−14.4	−3.2	−14.4	+0.6	8.4	−2.0
		−2.8 (av)		+0.4 (av)		−1.8 (av)

$B_{10}H_{14}$, whose B(1,3) and B(6,9) nuclei exhibit ^{11}B solvent shifts of as much as 1.3 ppm. More typical, however, is the *nido*-carborane 2,3-$(C_2H_5)_2C_2B_4H_6$ (Figure 1a), whose shifts ($\Delta\delta$) in a variety of solvents are no larger than 0.5 ppm with respect to a solution in *n*-hexane employed as a standard (Table I).

The situation is markedly different when one or more transition-metal atoms are present in the boron framework, as in metallaboranes and metallacarboranes. In our laboratory we have noted for some time that the spectra of such compounds often vary significantly in different solvents and, moreover, that the effect is selective based on the locations of boron nuclei in the framework. In an effort to more systematically document this phenomenon, we measured the high-resolution (115.8-MHz) ^{11}B FT NMR spectra of a series of structurally established molecules shown in

(3) In many published papers, NMR solvents are not even mentioned. In our view this information is a vital part of the experimental procedure and should be a prerequisite to publication.

(4) Gaines, D. F.; Nelson, C. K.; Kunz, J. C.; Morris, J. H.; Reed, D. *Inorg. Chem.* **1984**, *23*, 3252.

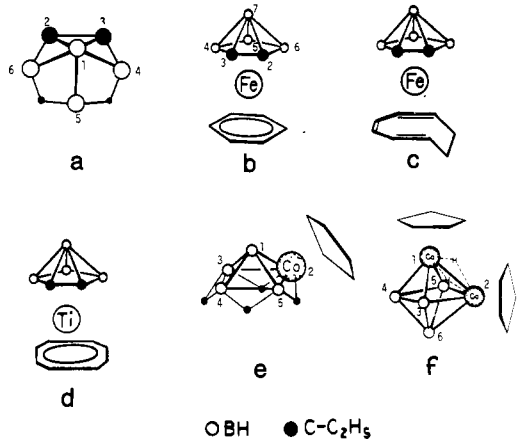

Figure 1. Molecular structures of (a) *nido*-2,3-$(C_2H_5)_2C_2B_4H_6$, (b) *nido*-1,2,3-$(\eta^6$-$C_6H_6)Fe(C_2H_5)_2C_2B_4H_4$, (c) *nido*-1,2,3-$(\eta^6$-$C_8H_{10})Fe(C_2H_5)_2C_2B_4H_4$, (d) *nido*-1,2,3-$(\eta^8$-$C_8H_8)Ti(C_2H_5)_2C_2B_4H_4$, (e) *nido*-2-$(\eta^5$-$C_5H_5)CoB_4H_8$, and (f) *closo*-1,2-$(\eta^5$-$C_5H_5)_2Co_2B_4H_6$.

Table V. Solvent-Induced ^{11}B FT NMR Shifts for 1,2-$(\eta^5$-$C_5H_5)_2Co_2B_4H_6$

solvent	δ[B(3,5)]	Δδ	δ[B(4,6)]	Δδ
hexane	64.4		23.2	
benzene	63.4	−1.0	21.6	−1.6
diethyl ether	63.5	−0.9	22.0	−1.2
tetrahydrofuran	62.5	−1.9	20.9	−2.3
acetone	62.0	−2.4	20.2	−3.0
dichloromethane	61.6	−2.8	19.9	−3.3
chloroform	61.2	−3.2	19.5	−3.7
methanol	61.8	−2.6	20.0	−3.2
acetonitrile	61.4	−3.0	19.2	−4.0
		−2.2 (av)		−2.8 (av)

Figures 1b–f and list the results in Tables II–V. Two patterns are clearly evident in these data: the solvent shifts relative to *n*-hexane solutions are quite large (exceeding 3 ppm in some cases), and there is a strong correlation with molecular structure. Thus, the ferracarboranes 1,2,3-$(\eta^6$-$C_6H_6)Fe(C_2H_5)_2C_2B_4H_4$[5a] (Figure 1b) and 1,2,3-$(\eta^6$-$C_8H_{10})Fe(C_2H_5)_2C_2B_4H_4$[5b] (Figure 1c) display large solvent effects at the B(5) and B(7) positions but relatively small shifts at B(4,6), as shown in Table II. In the structurally related titanacarborane 1,2,3-$(\eta^5$-$C_8H_8)Ti(C_2H_5)_2C_2B_4H_4$[6] (Figure 1d), the effect at B(7) is smaller (Table III) even when one allows for the use of a benzene rather than hexane solution as the standard (the compound is insufficiently soluble in hexane). This observation may be related to weak titanium–carbon covalent bonding in this species, which is implied by an unusually long Ti–carborane vector distance (1.916 Å) in the crystallographically determined structure.[6] The pattern observed in the cobaltaborane 2-$(\eta^5$-$C_5H_5)CoB_4H_8$[7] (Figure 1e) is similar in that the largest shifts occur at the apex boron B(1) and the basal boron B(4) which is trans to the metal (Table IV). In the closo species 1,2-$(\eta^5$-$C_5H_5)_2Co_2B_4H_6$[8] (Figure 1f and Table V), large solvent shifts are observed for both types of boron nuclei, with those in the trans locations [B(4,6)] exhibiting a slightly larger effect.

The direction of the shifts appears significant in the metal-containing species. Thus, while the values of Δδ in $(C_2H_5)_2C_2B_4H_6$ are scattered, those of the iron complexes and of the dicobalt compound are, without exception, upfield with respect to hexane solution; in 2-$(\eta^5$-$C_5H_5)CoB_4H_8$, the shifts of the apical and trans basal borons [B(1) and B(4)] are consistently upfield but those of the adjacent basal borons [B(3,5)] are downfield in all solvents examined. In the titanium complex (Table III) the shifts with reference to benzene are similarly upfield except for the ether solution. The observation in most cases of increased shielding may indicate higher electron density at the boron nuclei (as would be expected since the solvents employed are better electron donors than *n*-hexane), but the paramagnetic term in Ramsey's equation is also a significant contributor to ^{11}B shielding. As one might anticipate, the solvents of high dielectric constant and coordinating ability (acetone, methanol, acetonitrile) induce large shifts. However, the greatest shifts most frequently (in our sample) occur in dichloromethane, a solvent possessing neither high dielectric constant nor Lewis basicity. It is possible that weak hydrogen bonding between CH_2Cl_2 and BH groups is induced by a transfer of electron density from boron nuclei toward the metal center.

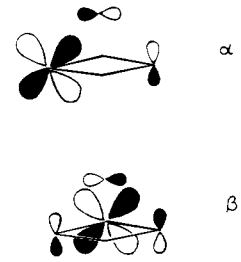

Figure 2. Metal (d_{xy} or d_{xz})–boron (p_x or p_z) bonding interactions in 2-$(\eta^5$-$C_5H_5)CoB_4H_8$. The Co–B(1)–B(4) and Co–B(1)–B(3,5) MOs are shown as α and β, respectively.[9]

In general, the data in Tables II–V can be correlated with previously described molecular orbital models for metal–boron clusters. Self-consistent charge calculations[9] on 2-$(\eta^5$-$C_5H_5)$-CoB_4H_8 indicated that the highest occupied bonding MOs are those designated α and β in Figure 2. The α MO furnishes good overlap between Co and the apex [B(1)] and trans [B(4)] borons, while β provides only weak bonding between the metal and its adjacent boron atoms [B(3,5)].[9] If this model is at least qualitatively correct, solvent-induced shielding in the vicinity of the metal may be selectively communicated to B(1) and B(4) via the α MO, consistent with the observation of a large solvent effect at those sites. (Alternatively, the effect of the metal-containing (α and β) MOs may be to increase the susceptibility of selected boron nuclei to *direct* influence by the solvent; the available data do not distinguish between these scenarios.) This idea is reminiscent of Burg's argument[10] accounting for the large ^{11}B shielding at the trans [B(4)] boron atoms in 2-halopentaborane(9) (2-XB_5H_8, X = F, Cl, Br), which utilizes B_5H_9 MOs calculated by Eberhardt, Crawford, and Lipscomb.[11] In these derivatives the effect of halogen substitution at a basal (2) position is felt most strongly at the trans [B(4)] location, an effect that is proposed to be transmitted through an MO analogous to α in the 2-$(\eta^5$-$C_5H_5)CoB_4H_8$ system. A more recent paper by Todd et al. extended Burg's observations to include metallaboranes and presented evidence for antipodal shielding effects.[12] A case of antipodal–vicinal differentiation which resembles that in 2-$(\eta^5$-$C_5H_5)CoB_4H_8$ has been observed in a series of carboranes by Hermanek et al., who suggest that the vicinal shifts (produced by substituents on the boron framework) follow an inductive mechanism and are related to the electronegativity of their substituents.[13] This is different from the antipodal effect, however, and in 2-$(\eta^5$-$C_5H_5)CoB_4H_8$ it is likely that both types of mechanisms, are reflected in the observed shifts.

In the metallacarboranes in Figure 1b–d, a similar qualitative argument can be presented, suggesting that the electronic interaction of iron with B(5) and B(7) is stronger than that with B(4) and B(6) on the basis of orbital overlap considerations. However,

(5) (a) Swisher, R. G.; Sinn, E.; Grimes, R. N. *Organometallics* **1983**, *2*, 506. (b) Maynard, R. B.; Swisher, R. G.; Grimes, R. N. *Ibid.* **1983**, *2*, 500.
(6) Swisher, R. G.; Sinn, E.; Grimes, R. N. *Organometallics* **1984**, *3*, 599.
(7) Venable, T. L.; Sinn, E.; Grimes, R. N. *J. Chem. Soc., Dalton Trans.* **1984**, 2275 and references therein.
(8) Pipal, J. R.; Grimes, R. N. *Inorg. Chem.* **1979**, *18*, 252.
(9) Brint, P.; Spalding, T. R. *J. Chem. Soc., Dalton Trans.* **1980**, 1236.
(10) Burg, A. B. *J. Am. Chem. Soc.* **1968**, *90*, 1407.
(11) Eberhardt, W. H.; Crawford, B.; Lipscomb, W. N. *J. Chem. Phys.* **1954**, *22*, 989.
(12) Siedle, A. R.; Bodner, G. M.; Garber, A. R.; Beer, D. C.; Todd, L. J. *Inorg. Chem.* **1974**, *13*, 2321.
(13) Hermanek, S.; Gregor, V.; Stibr, B.; Plesek, J.; Janousek, Z.; Antonovich, V. A. *Collect. Czech. Chem. Commun.* **1976**, *41*, 1492.

to our knowledge detailed molecular orbital calculations on *closo*-MC_2B_4 cage systems are not yet available (although the hypothetical borane analogue $Fe(\eta^5\text{-}B_6H_6)_2^{6-}$ has been examined[14]). In any event, the close similarity observed for the species examined in this study points to a common shielding mechanism in which the metal plays a major role.

Experimental Section

The carboranes and metallaboron cluster compounds examined were obtained via procedures described in the references cited, and all solutions were prepared from dried solvents. Concentrations of each compound in different solvents were held constant by employing the same solid sample and dissolving in an identical volume of each solvent. Corrections for bulk diamagnetic susceptibilities were not made.[15] Boron-11 FT NMR spectra at 115.8 MHz were recorded at 25 ± 1 °C on a Nicolet Magnetics Corp. NT-360/Oxford spectrometer, and data manipulation utilized standard Nicolet software with a 1280/293B data system. Spectra were recorded unlocked in a stable (measured drift rate $<2 \times 10^{-3}$ Hz/h) magnetic field (8.5 T). Referencing was to an external solution of $BF_3{\cdot}O(C_2H_5)_2$. Uninterrupted, incoherent ^1H decoupling at low levels (~2 W) was employed.

Acknowledgment. This work was supported in part by the National Science Foundation, Grant No. 81-19936.

(14) Calhorda, M. J.; Mingos, D. M. P. *J. Organomet. Chem.* **1982**, *229*, 229.
(15) Corrections for bulk susceptibility are seldom, if ever applied in ^{11}B NMR spectroscopy owing to the small effects (less than normal line widths) and the relatively large uncertainty in the calculated corrections (cf: Bothner-By, R. E.; Glick, A. K. *J. Chem. Phys.* **1957**, *26*, 1647).

Contribution No. 7167 from the
Arthur Amos Noyes Laboratories,
Division of Chemistry and Chemical Engineering,
California Institute of Technology, Pasadena, California 91125

Relation between the Reduction Potentials of Adsorbed and Unadsorbed Cobalt(III) Tetrakis(*N*-methylpyridinium-4-yl)porphyrin and Those Where It Catalyzes the Electroreduction of Dioxygen

Ching-Long Ni and Fred C. Anson*

Received April 1, 1985

Most commonly, monomeric cobalt porphyrins, CoP, are irreversibly adsorbed on graphite or carbon electrodes and catalyze the electroreduction of O_2 to H_2O_2 at potentials significantly more negative than the formal potential of the $Co^{III/II}$ couple for the adsorbed porphyrin.[1,2] This observation is most simply explained by a catalytic mechanism in which the reduction of the cobalt center of the porphyrin from Co(III) to Co(II) is not coupled to the catalytic cycle. The latter involves coordination of O_2 to the reduced cobalt center followed by the reduction of the adduct at potentials determined by its electrochemical properties rather than those of the original cobalt porphyrin.[2] This mechanistic scheme has accommodated the results we have obtained with a series of monomeric cobalt porphyrins.[1,2] However, the Co(III/II) formal potential for cobalt tetrakis(*N*-methylpyridinium-4-yl)porphyrin, CoTMPyP, evaluated recently by Rohrbach et al.[3] (0.175 V vs. SCE) is more negative, instead of more positive, than the potential where this porphyrin catalyzes the reduction of O_2, (~0.25 V).

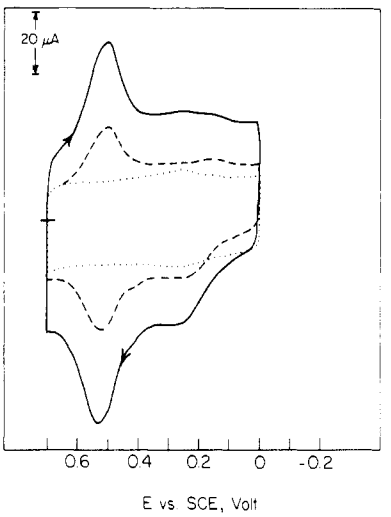

Figure 1. Steady-state cyclic voltammetry of 0.2 mM CoTMPyP in 0.5 M CF_3COOH saturated with argon (dotted curve no CoTMPyP present). Scan rates: dashed curve and dotted curve, 100 mV s^{-1}; solid curve, 200 mV s^{-1}.

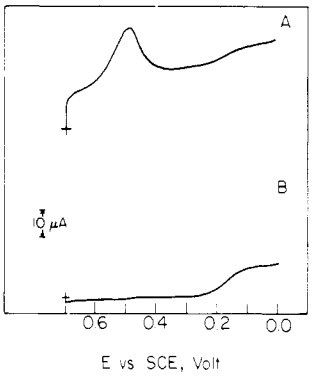

Figure 2. (A) Non-steady-state current–potential response obtained with a rotating disk electrode in the solution used to record Figure 1 (rotation rate 400 rpm; potential scanned at 100 mV s^{-1}). (B) Repeat of part A under steady-state conditions. Potential scan rate = 0 mV s^{-1}.

The origin of this apparently dissimilar behavior was traced to an unusually large change in the formal potential of the $Co^{III/II}$ couple upon the adsorption of the porphyrin on the graphite-electrode surface. The purpose of this note is to draw attention to the magnitude of the shifts in cobalt porphyrin formal potentials that their adsorption on electrode surfaces can produce and to assess its significance on the mechanism of the catalyzed reduction of O_2.

Experimental Section

$[Co^{II}TMPyP](PF_6)_4$ was prepared as previously described[4] and purified according to the procedure of Kobayashi et al.[5] $Co^{III}TMPyP$ was generated by controlled-potential oxidation at 0.6 V at a graphite-plate electrode.

The electrochemical apparatus, instrumentation, and procedures were similar to those previously described.[6,7] The working electrodes were cylindrical pyrolytic graphite rods mounted to expose the edges of the graphite planes (Union Carbide Co., Chicago). They were polished with No. 600 SiC paper (3M Co., Minneapolis, MN) and mounted as described previously.[2] Measurements were conducted at 22 ± 2 °C with solutions prepared from distilled water that had been passed through a purification train (Barnsted Nanopure + Organopure). Potentials are given with respect to a saturated calomel electrode, SCE.

(1) Durand, R. R., Jr. Ph.D. Thesis, California Institute of Technology, 1984.
(2) Durand, R. R., Jr.; Anson, F. C. *J. Electroanal. Chem. Interfacial Electrochem.* **1982**, *134*, 273.
(3) Rohrbach, D. F.; Deutsch, E.; Heineman, W. R.; Pasternack, R. F. *Inorg. Chem.* **1977**, *16*, 2650.
(4) Anson, F. C.; Ni, C.-L.; Saveant, J. M. *J. Am. Chem. Soc.* **1985**, *107*, 3442.
(5) Kobayashi, N.; Fujihira, M.; Osa, T.; Kuwana, T. *Bull. Chem. Soc. Jpn.* **1980**, *53*, 2195.
(6) Oyama, N.; Anson, F. C. *Anal. Chem.* **1980**, *52*, 1192.
(7) Geiger, T.; Anson, F. C. *Anal. Chem.* **1980**, *52*, 2448.

0020-1669/85/1324-4754$01.50/0